LINEAR INTERFACE CRACK UNDER HARMONIC SHEAR: EFFECTS OF CRACK'S FACES CLOSURE AND FRICTION

OLEKSANDR V. MENSHYKOV[1*], VASYL A. MENSHYKOV[2], IGOR A. GUZ[1] AND MARINA V. MENSHYKOVA[1]

[1]Centre for Micro- and Nanomechanics, School of Engineering, University of Aberdeen, AB24 3UE Aberdeen, Scotland, UK

[2] National Aerospace University – "Kharkiv Aviation Institute" Chkalova St, 17, Kharkiv 61000, Ukraine

Key words: Interface Crack, Boundary Integrals, Harmonic Shear, Crack Closure and Friction.

Summary. The linear crack between two dissimilar elastic isotropic half-spaces under normal harmonic shear loading is considered taking the crack's faces contact interaction and friction into account. The problem is solved by the boundary integral equations method and the components of the solution are represented by the Fourier series. The numerical convergence of the method is analysed. The results are validated through the comparison with the classical model solutions obtained for the static problems with and without friction. The effects of material properties and values of the friction coefficient on the distribution of the stress intensity factors (normal opening and transverse shear modes) are presented and analysed.

[*]Corresponding author. Tel.: +44 1224 273326; fax: +43 1224 272519;

e-mail: o.menshykov@abdn.ac.uk

1 INTRODUCTION

The understanding of the fracture mechanisms and deterioration of the material properties are the questions of great interest for engineering science and industry. As all materials have crack-like defects, the problems of stress concentrations and cracks' propagations are of high attention [1–6].

Nowadays the use of composite materials is continuously increasing, the fracture mechanics problems for interlaminar cracks under different types of loading are very important, as, for example, it was underlined by Comninou in the overview of interface cracks under static loading [2]. In the previous studies the interface cracks under shear loading [3, 4], and combined tension-compression and shear [5] allowing the partial closure of the crack faces were considered. Linear cracks between homogeneous isotropic materials under static loading were also considered in [7], where the new algorithm for J_k-integrals evaluation, which can be used for stress intensity factors' estimation, was presented. The suggested method may also be extended for the case of curvilinear interface cracks.

The boundary element method was employed for the stress intensity factors' evaluation in [8], where the crack between two anisotropic materials under static loading was considered and the recommendations on the choice of the optimal boundary element analysis approach were given.

Paper [9] presented the use of Galerkin method to solve the dynamic loading problems. In the solution the crack faces contact interaction was taken into account and the results for the linear crack under normal tension-compression loading were obtained. The use of boundary integral equations to solve the interface cracks' contact problems were considered in a number of publications [10–15]. In [10] the multi-parametric iterative algorithm for the solution of interface crack problems was

presented, the investigation of the algorithm convergence was carried out, and the effects of frequency for the linear interface crack under tension-compression load were also studied. The numerical solutions of two- and three-dimensional interface crack dynamic problems were presented in [11–15].

Advanced boundary integral equations method may also be used for the wave propagation problem solution. Using this method the problem for layered piezoelectric phononic crystals with cracks was solved in [16]. Integral equations with hypersingular kernels were applied for the solution of fracture mechanics problems in [17]. A semi-analytical approach, namely the scaled boundary finite element method, was used to model crack face contact and propagation problems in [18–20]. The high-order completeness analysis of the method was provided in [21].

Problems for the penny-shaped crack in between the half-space and thin top layer under static and dynamic time-harmonic horizontal loading were investigated in [22]. Coupled dual integral equations were solved analytically for the case of static loading and numerically for the dynamic loading. In the static case, transversely isotropic linear elastic materials were considered, when for the dynamic case the problem was solved for the isotropic materials only. The influence of the degree of anisotropy and the thickness of the top layer on the problem solution was studied in details. Array of penny-shaped cracks under time-harmonic loading was considered in [23, 24]. Improved boundary integral equation method was used for the investigation of the wave propagation [23] and computation of the dynamic stress distrubutions [24].

Cracks in Functionally Graded Materials (FGMs) were considered in [25–29]. In-plane harmonic load of the FGM with multiple cracks was investigated in [25], where the influence of different parameters on the dynamic stress intensity factors was analysed. The problems for the cracks located on the interface of two dissimilar half-

planes were solved in [26–29]. Functionally graded magnetoelastic solid with cracks under time-harmonic SH-waves was considered in [30], where the problems for arbitrary direction of wave propagation were solved and the effects of the inhomogeneity of the material were analysed using boundary integral equations method.

Two-dimensional decagonal quasicrystal bimaterial with the interface crack was studied in [31]. The general solution and Fourier transition were used to obtain the fundamental solution for the extended displacement discontinuity method. Using the proposed method the extended stress intensity factors were obtained. The verification of the method was done by comparing the obtained results for phonon and phason stresses with the ones received for the numerical COMSOL model.

Interface cracks in one-dimensional hexagonal quasi-crystal coating under in-plane loading were considered in [32]. For the numerical simulation the authors used the displacement discontinuity boundary element method, presenting the comprehensive analysis of the influence of coating thickness, material properties and crack length on the fracture behaviour, distribution of stress intensity factors and energy release rates.

Mode III interface crack problems were considered in [33], where the overview of the problems' solutions was given. In the study the dependencies of the stress intensity factors and energy release rates on the bimaterial constants were discussed. In particular, the problem of the interaction between the interface linear crack and internal micro-cracks under anti-plane shear loading was solved using singular integral equations. Using the suggested solution the conditions under which internal micro-cracks do not influence the distribution of the stress intensity factors for the interface crack can be found.

The problem of semi-infinite interface crack in poroelastic strip under shear wave

was investigated in [34]. To obtain the stress intensity factors the Fourier integral transform and the Wiener-Hopf method were used. The detailed study of thickness ratio, porosity, stress amplitude ratio and inhomogeneity parameters influence on stress intensity factors was conducted. The semi-strip with a longitudinal crack was considered in [35], using two different approaches and comparing the stress intensity factors computed for both models. Crack on the interface of dissimilar orthotropic strips was investigated in [36]. The problem for the crack under dynamic anti-plane shear traction was solved analytically, using separation of variables technique and reducing the problem to a singular integral equation.

Interfacial crack under impact loading was considered in [37–42]. Comparison of two hypersingular time domain boundary element methods for 2-D cracks under transient dynamic loading was done by Wuensche et al. [37]. Sawtooth shock pulse problem was solved by Zhang et al. [38]. A crack on the interface of orthotropic materials under impact loading was considered in [39]. The problems of penny-shaped cracks (within the layer and on the layers' interface) under impact of torsional load were solved in [40, 41]. In [42] the problem for three parallel cracks under normal impact loading was investigated.

The interface linear and penny-shaped cracks under harmonic shear loading were considered in [43, 44]. The problems were solved by boundary element method using the system of boundary singular integral equations. Displacements and tractions distributions on the bimaterial interface were analysed. Also, the stress intensity factors for different wave numbers were obtained. We must note that these problems were solved neglecting the crack faces contact interaction. Despite that under some conditions the problem may be solved correctly with this assumption (for example, for cracks with considerable initial opening), in the general case the crack faces contact

interaction must be taken into account to obtain the realistic stress-strain state.

In the conference proceeding [45] the analysis of the size of the contact zone was presented for a linear interface crack under the normal harmonic shear loading. The problem was solved using the iterative correction algorithm in order to take the crack closure and the friction of the crack's faces into account. The displacements and contact forces at the crack faces were presented and analysed for a fixed value of the wave number and a fixed value of the friction coefficient, but the stress intensity factors were not computed.

The current study is devoted to the parametric analysis of the effects of the crack closure and friction on stress intensity factors (normal opening and transverse shear modes) for a linear interface crack under normal harmonic shear. The numerical convergence of the iterative solution algorithm is analysed for various iterative coefficients. The results are validated through the comparison with the classical model solutions by Comninou and Dundurs obtained for the static problems with and without friction [4]. The effects of material's properties and values of the friction coefficient on the distribution of the stress intensity factors for the first time are presented and analysed for various bi-materials. It was noted that the changes in material's properties led to the significant changes in the magnitudes of the stress intensity factors and the frequencies at which the maximums are achieved. Furthermore, the effects of the friction become more important (in particular, for the transverse shear mode) for higher ratios between elastic properties of the bi-material constituents.

2 STATEMENT OF THE PROBLEM

Let us consider an elastic bimaterial consisting of two homogeneous isotropic half-spaces, $\Omega^{(1)}$ and $\Omega^{(2)}$, with the crack of finite length $2L$ located at the interface between

half-spaces. The crack has no initial opening, and the normal mono-harmonic shear loading with the frequency of $\omega = 2\pi/T$ is applied to the material [43, 45] (Figure 1).

In both half-spaces the equation of motion and the generalized Hooke's law lead to the linear Lamé equations of elastodynamics for the displacement field with the standard initial and boundary conditions for displacements and stresses (namely, no initial deformations of the material; the Sommerfeld radiation-type condition at the infinity; continuity conditions for stresses and displacements at the bonding interface, $\Gamma^* = \Gamma^{(1)} \cap \Gamma^{(2)}$; and known initial tractions at the crack opposite faces, $\Gamma^{(1)cr}$ and $\Gamma^{(2)cr}$, caused by the incident external loading, $\mathbf{g}(\mathbf{x}, t)$).

The components of the displacement field could be represented by the displacements $\mathbf{u}(\mathbf{x}, t)$ and tractions $\mathbf{p}(\mathbf{x}, t)$ at the half-spaces' boundaries, $\Gamma^{(1)}$ and $\Gamma^{(2)}$, using the Somigliana dynamic identity with the appropriate fundamental solutions $U_{ij}^{(m)}(\mathbf{x}, \mathbf{y}, t-\tau)$ and $W_{ij}^{(m)}(\mathbf{x}, \mathbf{y}, t-\tau)$ [1, 10, 46–48]:

$$u_j^{(m)}(\mathbf{x}, t) = \int_T \int_{\Gamma^{(m)}} (p_i^{(m)}(\mathbf{y}, \tau) U_{ij}^{(m)}(\mathbf{x}, \mathbf{y}, t-\tau) - u_i^{(m)}(\mathbf{y}, \tau) W_{ij}^{(m)}(\mathbf{x}, \mathbf{y}, t-\tau)) d\mathbf{y} d\tau, \quad \mathbf{x} \in \Omega^{(m)}, \quad t \in T, \quad j=1,2, \tag{1}$$

where $T = 0; +\infty$ is the time interval (period of the harmonic loading for the case of harmonic incident wave).

Due to the crack's faces closure the traction vector at the crack's surface is the superposition of the known initial traction caused by the external loading and the contact force, $\mathbf{q}(\mathbf{x}, t)$, that appears in the contact zone, thus $\mathbf{p}(\mathbf{x}, t) = \mathbf{g}(\mathbf{x}, t) + \mathbf{q}(\mathbf{x}, t)$. The size and shape of the contact zone in time are unknown beforehand, depend on the parameters of the external loading (type of the loading, direction, magnitude,

frequency, etc.), mechanical properties of the bi-material and the friction coefficient at the crack's surface and must be determined during the solution process.

To include the contact interaction into account, the Signorini unilateral constraints and the Coulomb friction law with the friction coefficient k_τ must be imposed for the normal and tangential components of the displacement discontinuity, $[\mathbf{u}(\mathbf{x},t)] = \mathbf{u}^{(1)}(\mathbf{x},t) - \mathbf{u}^{(2)}(\mathbf{x},t)$, and contact forces [47, 48]:

$$[u_n(\mathbf{x},t)] \geq 0, \quad q_n(\mathbf{x},t) \geq 0, \quad [u_n(\mathbf{x},t)]q_n(\mathbf{x},t) = 0, \tag{2}$$

$$| q_\tau(\mathbf{x},t) | < k_\tau q_n(\mathbf{x},t) \Rightarrow \frac{\partial [u_\tau(\mathbf{x},t)]}{\partial t} = 0, \tag{3}$$

$$| q_\tau(\mathbf{x},t) | = k_\tau q_n(\mathbf{x},t) \Rightarrow \frac{\partial [u_\tau(\mathbf{x},t)]}{\partial t} = -\frac{q_\tau(\mathbf{x},t)}{|q_\tau(\mathbf{x},t)|}\left|\frac{\partial [u_\tau(\mathbf{x},t)]}{\partial t}\right|. \tag{4}$$

The contact constraints (2)–(4) ensure that there is no interpenetration of the opposite crack faces, the normal component of the contact force is unilateral and present in the contact zone only; and the opposite crack faces do not move in the tangential plane while they are held by the friction force before the slipping happens [10, 12, 45, 47].

Contact interaction makes the problem highly non-linear and the solution is cyclic multi-harmonic even for the considered case of mono-harmonic loading. That is why the normal and tangential components of the displacement discontinuity and the traction at the crack surface can be approximated by the following exponential Fourier series with respect to time [10, 12, 45, 47]:

$$f(\bullet,t) = Re\left\{\sum\nolimits_{k=-\infty}^{+\infty} f^k(\bullet) e^{I\omega_k t}\right\}, \quad f^k(\bullet) = \frac{\omega}{2\pi}\int_0^T f(\bullet,t) e^{-I\omega_k t}\, dt, \tag{5}$$

where $\omega_k = 2\pi k/T$ and I is the imaginary unit.

Assuming that the distributions of the boundary displacements and tractions are smooth enough, after the limiting transition to the interface the Somigliana integral

identity in time domain (1) may be transformed into the following system of boundary integral equations in the frequency domain [10, 12, 45]:

$$-\int_{\Gamma^{(1)\mathrm{cr}}} \tilde{p}_i^{k,(1)}(\mathbf{y}) U_{ij}^{(1)}(\mathbf{x},\mathbf{y},\omega_k) d\mathbf{y} = -\frac{1}{2} u_i^{k,(1)}(\mathbf{x}) - \int_{\Gamma^{(1)\mathrm{cr}}} u_i^{k,(1)}(\mathbf{y}) W_{ij}^{(1)}(\mathbf{x},\mathbf{y},\omega_k) d\mathbf{y} + \int_{\Gamma^*} u_i^{k,*}(\mathbf{y}) W_{ij}^{(1)}(\mathbf{x},\mathbf{y},\omega_k) d\mathbf{y} - \int_{\Gamma^*} p_i^{k,*}(\mathbf{y}) U_{ij}^{(1)}(\mathbf{x},\mathbf{y},\omega_k) d\mathbf{y}, \quad \mathbf{x} \in \Gamma^{(1)\mathrm{cr}}, \tag{6}$$

$$-\int_{\Gamma^{(2)\mathrm{cr}}} \tilde{p}_i^{k,(2)}(\mathbf{y}) U_{ij}^{(2)}(\mathbf{x},\mathbf{y},\omega_k) d\mathbf{y} = -\frac{1}{2} u_i^{k,(2)}(\mathbf{x}) - \int_{\Gamma^{(2)\mathrm{cr}}} u_i^{k,(2)}(\mathbf{y}) W_{ij}^{(2)}(\mathbf{x},\mathbf{y},\omega_k) d\mathbf{y} - \int_{\Gamma^*} u_i^{k,*}(\mathbf{y}) W_{ij}^{(2)}(\mathbf{x},\mathbf{y},\omega_k) d\mathbf{y} + \int_{\Gamma^*} p_i^{k,*}(\mathbf{y}) U_{ij}^{(2)}(\mathbf{x},\mathbf{y},\omega_k) d\mathbf{y}, \quad \mathbf{x} \in \Gamma^{(2)\mathrm{cr}}, \tag{7}$$

$$-\int_{\Gamma^{(1)\mathrm{cr}}} \tilde{p}_i^{k,(1)}(\mathbf{y}) U_{ij}^{(1)}(\mathbf{x},\mathbf{y},\omega_k) d\mathbf{y} = -\frac{1}{2} u_i^{k,*}(\mathbf{x}) - \int_{\Gamma^{(1)\mathrm{cr}}} u_i^{k,(1)}(\mathbf{y}) W_{ij}^{(1)}(\mathbf{x},\mathbf{y},\omega_k) d\mathbf{y} + \int_{\Gamma^*} u_i^{k,*}(\mathbf{y}) W_{ij}^{(1)}(\mathbf{x},\mathbf{y},\omega_k) d\mathbf{y} - \int_{\Gamma^*} p_i^{k,*}(\mathbf{y}) U_{ij}^{(1)}(\mathbf{x},\mathbf{y},\omega_k) d\mathbf{y}, \quad \mathbf{x} \in \Gamma^*, \tag{8}$$

$$-\int_{\Gamma^{(2)\mathrm{cr}}} \tilde{p}_i^{k,(2)}(\mathbf{y}) U_{ij}^{(2)}(\mathbf{x},\mathbf{y},\omega_k) d\mathbf{y} = -\frac{1}{2} u_i^{k,*}(\mathbf{x}) - \int_{\Gamma^{(2)\mathrm{cr}}} u_i^{k,(2)}(\mathbf{y}) W_{ij}^{(2)}(\mathbf{x},\mathbf{y},\omega_k) d\mathbf{y} - \int_{\Gamma^*} u_i^{k,*}(\mathbf{y}) W_{ij}^{(2)}(\mathbf{x},\mathbf{y},\omega_k) d\mathbf{y} + \int_{\Gamma^*} p_i^{k,*}(\mathbf{y}) U_{ij}^{(2)}(\mathbf{x},\mathbf{y},\omega_k) d\mathbf{y}, \quad \mathbf{x} \in \Gamma^*, \tag{9}$$

where $\tilde{p}_i^{k,(m)}(\mathbf{x})$, $p_i^{k,*}(\mathbf{x})$, $u_i^{k,(m)}(\mathbf{x})$ and $u_i^{k,*}(\mathbf{x})$ are the Fourier coefficients of the tractions and displacements at the crack's faces and the bonding interface.

Fundamental solutions in the frequency domain $U_{ij}^{(m)}(\mathbf{x},\mathbf{y},\omega_k)$ and $W_{ij}^{(m)}(\mathbf{x},\mathbf{y},\omega_k)$ have the following form [1, 21, 46, 47]:

$$U_{ij}^{(m)}(\mathbf{x},\mathbf{y},\omega_k) = \frac{1}{2\pi\mu^{(m)}}\left(\psi_k^{(m)}\delta_{ij} - \chi_k^{(m)}\frac{(y_i - x_i)}{r}\frac{(y_j - x_j)}{r}\right), \tag{10}$$

$$W_{ij}^{(m)}(\mathbf{x},\mathbf{y},\omega_k) = \lambda^{(m)} n_i^{(m)}(\mathbf{y}) \frac{\partial}{\partial y_k} U_{kj}^{(m)}(\mathbf{x},\mathbf{y},\omega_k) + \mu^{(m)} n_k^{(m)}(\mathbf{y}) \left[\frac{\partial}{\partial y_k} U_{ij}^{(m)}(\mathbf{x},\mathbf{y},\omega_k) + \frac{\partial}{\partial y_i} U_{kj}^{(m)}(\mathbf{x},\mathbf{y},\omega_k)\right]. \tag{11}$$

Here δ_{ij} is the Kronecker delta, $\lambda^{(m)}$ and $\mu^{(m)}$ are the Lamé coefficients, $r = |x_1 - y_1|$ is the distance between the observation and load points (please note that the

displacements of the crack faces are negligibly small comparing to the distance between observation and load points along the crack length).

Functions $\psi_k^{(m)}$ and $\chi_k^{(m)}$ for the harmonic loading in two-dimensional case are given as:

$$\psi_k^{(m)} = K_0(l_{2,k}^{(m)}) + \frac{1}{l_{2,k}^{(m)}}\left[K_1(l_{2,k}^{(m)}) - \frac{c_2^{(m)}}{c_1^{(m)}}K_1(l_{1,k}^{(m)})\right],$$

$$\chi_k^{(m)} = K_2(l_{2,k}^{(m)}) - \left(\frac{c_2^{(m)}}{c_1^{(m)}}\right)^2 K_2(l_{1,k}^{(m)}), \tag{12}$$

where $l_{1,k}^{(m)} = I\omega k\, r/c_1^{(m)}$, $l_{2,k}^{(m)} = I\omega k\, r/c_2^{(m)}$; $K_n(\bullet)$ is the modified Bessel function of the second kind and order n; and $c_1^{(m)} = \sqrt{(\lambda^{(m)} + 2\mu^{(m)})/\rho^{(m)}}$ and $c_2^{(m)} = \sqrt{\mu^{(m)}/\rho^{(m)}}$ are the velocities of the longitudinal and transversal waves in the upper and lower half-spaces.

For the considered case the integral kernels $U_{ij}^{(m)}(\mathbf{x}, \mathbf{y}, \omega_k)$ and $W_{ij}^{(m)}(\mathbf{x}, \mathbf{y}, \omega_k)$ have the following form:

$$U_{12}^{(m)}(\mathbf{x}, \mathbf{y}, \omega_k) = U_{21}^{(m)}(\mathbf{x}, \mathbf{y}, \omega_k) = 0, \tag{13}$$

$$U_{11}^{(m)}(\mathbf{x}, \mathbf{y}, \omega_k) = \frac{1}{2\pi\mu^{(m)}}\left[K_0\left(l_{2,k}^{(m)}\right) + \frac{1}{l_{2,k}^{(m)}}\left(K_1\left(l_{2,k}^{(m)}\right) - \frac{c_2^{(m)}}{c_1^{(m)}}K_1\left(l_{1,k}^{(m)}\right)\right)\right], \tag{14}$$

$$U_{22}^{(m)}(\mathbf{x}, \mathbf{y}, \omega_k) = \frac{1}{2\pi\mu^{(m)}}\left[\left(\frac{c_2^{(m)}}{c_1^{(m)}}\right)^2 K_2\left(l_{1,k}^{(m)}\right) - K_2\left(l_{2,k}^{(m)}\right) + K_0\left(l_{2,k}^{(m)}\right) + \right.$$

$$\left. \frac{1}{l_{2,k}^{(m)}}\left(K_1\left(l_{2,k}^{(m)}\right) - \frac{c_2^{(m)}}{c_1^{(m)}}K_1\left(l_{1,k}^{(m)}\right)\right)\right], \tag{15}$$

$$W_{11}^{(m)}(\mathbf{x}, \mathbf{y}, \omega_k) = W_{22}^{(m)}(\mathbf{x}, \mathbf{y}, \omega_k) = 0, \tag{16}$$

$$W_{12}^{(m)}(\mathbf{x}, \mathbf{y}, \omega_k) = \frac{1}{2\pi r}\frac{\partial r}{\partial y_1}\left[l_{2,k}^{(m)}K_1\left(l_{2,k}^{(m)}\right) - 2K_2\left(l_{2,k}^{(m)}\right) + 2\left(\frac{c_2^{(m)}}{c_1^{(m)}}\right)^2 K_2\left(l_{1,k}^{(m)}\right)\right], \tag{17}$$

$$W_{21}^{(m)}(\mathbf{x}, \mathbf{y}, \omega_k) = \frac{1}{2\pi r}\frac{\partial r}{\partial y_1}\left[-\frac{\lambda^{(m)}\mu^{(m)}}{\left(\lambda^{(m)}+2\mu^{(m)}\right)^2}l_{1,k}^{(m)}K_1\left(l_{1,k}^{(m)}\right) - 2K_2\left(l_{2,k}^{(m)}\right) + 2\left(\frac{c_2^{(m)}}{c_1^{(m)}}\right)^2 K_2\left(l_{1,k}^{(m)}\right)\right]. \tag{18}$$

For every Fourier coefficient number, k, the appropriate system of linear algebraic equations (similar to the one presented in [13]) can be obtained from the system of boundary integral equations (6)–(9) and solved numerically, so the displacements and tractions in the form of Fourier exponential series (5) with a finite number of the members can be found. Note also that hypersingular, singular and weakly singular divergent integrals depending on the type and order of the used space approximation shall be regularised and calculated for all integral kernels. In the current study the simplest piecewise-constant approximation was used (as it successfully proved its efficiency for two-dimensional problems comparing, for example, with the Galerkin method [9]).

In order to take the contact constraints (2)–(4) into account the iterative correction algorithm based on the orthogonal projections on the sets of constraints shall be used. The detailed description, studies on the numerical convergence and the comparison of the iterative algorithms applicable to homogeneous and layered materials are given in [10, 47, 48], in the current study the following algorithm presented in [10] is used:

- the mono-harmonic solution of the problem neglecting the effects of the crack's closure and friction is obtained;
- the solution is corrected applying the contact constraints (2)–(4) and the Fourier coefficients are gradually changed until the multi-harmonic solution satisfying the contact constraints is found.

The detailed investigation of the algorithm's convergence with respect to the number of Fourier coefficients used in series (5), the number of the boundary elements (and size of the elements in the vicinity of the crack's tips) and the number of time intervals

has been presented in [10] for linear cracks in bimaterials under the harmonic tension-compression loading, thus in this study we followed the recommendations given in [10].

3 VALIDATION OF THE MODEL

For the validation of the numerical model the interface crack of the length $2L$ under the normal shear loading of amplitude σ_0 and the frequency closed to zero (with the normalised wave number $k_2^{(2)}L = \omega L/c_2^{(2)} = 0.01$) was considered [45]. The mechanical properties of the material ($\nu^{(1)} = 0.1$, $E^{(1)} = 29$ GPa, and $\nu^{(2)} = 0.49$, $E^{(2)} = 400$ GPa) were chosen to satisfy the following ratio [4]:

$$\beta = \frac{\mu^{(2)}\left(\kappa^{(1)} - 1\right) - \mu^{(1)}\left(\kappa^{(2)} - 1\right)}{\mu^{(2)}(\kappa^{(1)} + 1) + \mu^{(1)}(\kappa^{(2)} + 1)} = 0.5, \tag{19}$$

where $E^{(m)}$ is the Young's modulus, $\kappa^{(m)} = 3 - 4\nu^{(m)}$, and $\nu^{(m)}$ is the Poisson's coefficient.

The normal components of the displacement jump, $2\mu_0[u_n]/\sigma_0 L$, and contact forces, q_n/σ_0, at the crack surface are presented in Figures 2 and 3 for different values of the friction coefficient friction ($k_\tau = 0.0$ and $k_\tau = 1.0$), note that [43]:

$$\mu_0 = \mu^{(1)}\frac{1-\gamma_2}{1+\kappa^{(1)}}, \quad \gamma_2 = \frac{a_1}{2} - a_2,$$
$$a_1 = \frac{\mu^{(1)} - \mu^{(2)}}{\mu^{(1)} + \kappa^{(1)}\mu^{(2)}}, \quad a_2 = \frac{\kappa^{(1)}\mu^{(2)} - \kappa^{(2)}\mu^{(1)}}{2(\mu^{(2)} + \kappa^{(2)}\mu^{(1)})}. \tag{20}$$

The contact forces and the size of the contact zone are compared with the model static solution by Comninou and Dundurs [4]. As one can see the results are in a very good agreement. It should be noted that the friction significantly affected the solution, changing the size of the contact zone and the distribution of the displacements and

forces even for the “quasi-static” case considered in the present section for the validation purposes only.

Please note that as it was also shown in [45] after the correction the contact constraints (2)–(4) are satisfied on the entire surface of the crack (the most importantly, there are no interpenetration of the crack’s opposite faces and the friction is significantly affected the distribution of displacements and tractions, and the size of the contact zone), and the Sommerfeld conditions are satisfied at the infinity (the displacements and forces slowly but surely decrease at the bonding interface with the increase of the distance from the crack), so the iterative process effectively corrected the solution.

4 CASE STUDIES AND CONCLUSIONS

In order to be consistent with the results presented in [43] the mechanical properties of the bimaterial were taken as follows: the Poisson’s coefficient $\nu^{(1)} = \nu^{(2)} = 0.25$, density $\rho^{(1)} = \rho^{(2)} =$ 7800 kg/m^3, the Young’s modulus $E^{(1)} = 200$ GPa and $E^{(2)} = 150$ GPa, $E^{(2)} = 100$ GPa and, finally, $E^{(2)} = 67$ GPa.

The dynamic stress intensity factors (the opening and the transverse shear modes) were computed in the vicinity of the crack’s tip using the following asymptotic formulas [1, 43, 47]:

$$K_I^{max} = \max_t \lim_{r\to 0} p_n^*(R + r, t)\sqrt{2\pi r}, \tag{21}$$

$$K_{II}^{max} = \max_t \lim_{r\to 0} p_\tau^*(R + r, t)\sqrt{2\pi r}. \tag{22}$$

Here $p_n^*(R + r, t)$ and $p_\tau^*(R + r, t)$ are the normal and tangential components of the traction vector at the bonding interface and r is the distance from the crack tip.

Stress intensity factors (normal opening and transverse shear modes) plotted against the iteration number for different wave numbers at $\mu^{(2)}/\mu^{(1)} = 0.5$ and $k_\tau = 0.5$

are presented in Figures 4 and 5. The results are normalised by the appropriate static values. One can see a clear numerical convergence of the algorithm for different values of the iterative coefficient, K_n, that significantly affects the rate of the convergence.

Stress intensity factors (normal opening and transverse shear modes) plotted against the wave number at $\mu^{(2)}/\mu^{(1)} = 0.5$ and $k_\tau = 0.5$ are presented in Figures 6 and 7. It is obvious that the crack closure and friction significantly affect the solution for both modes of the stress intensity factor especially for higher wave numbers (higher frequencies of the loading). It shall be also noted that, based on the results presented in Figures 4–7, in order to achieve a stable convergence of the algorithm the iterative coefficient was fixed at $K_n = 2000$.

The effects of the friction coefficient on the distribution of the stress intensity factors are presented in Figures 8 and 9 at $\mu^{(2)}/\mu^{(1)} = 0.5$. It is clear that the change in the friction coefficient does not significantly affect the solution (the crack's faces are mostly sliding disregarding the friction coefficient value, because the friction force depending on the normal component of the contact force is quite small for the shear load considered here), so the correction of the crack's normal opening according to the Signorini unilateral constraints (2) mainly led to the change in both modes of the stress intensity factor. Note that this conclusion significantly varies from the ones obtained previously for the tension-compression waves where the normal opening for obvious reasons was the dominant mode [10, 12, 15].

Finally, the distribution of the stress intensity factors for different combinations of the materials properties is presented in Figures 10 and 11. It was noted that the changes in material's properties led to the significant changes in the magnitudes of the stress intensity factors and the frequencies at which the maximums are achieved. It may be also concluded that the discrepancy in the mechanical properties significantly

increases the effects of the cracks closure and friction especially for the transverse shear mode.

As a conclusion, it shall be added that the proposed approach may be extended to three-dimensional fracture mechanics problems for cracked materials under arbitrary dynamic loading, and the special attention shall be paid to the coupling oscillation singularities in the vicinity of the crack's front [2, 5, 49, 50].

REFERENCES

[1] Aliabadi MH, Brebbia CA, Parton VZ. (Eds.) Static and Dynamic Fracture Mechanics. Computational Mechanics Publications; 1994.

[2] Comninou M. An overview of interfacial cracks. Eng Fract Mech 1990; 37(1):197–208.

[3] Comninou M. The interface crack in a shear field. J App Mech 1978;45:287–290.

[4] Comninou M, Dundurs J. Effect of friction on the interface crack loaded in shear. J Elast 1980; 10:203–212.

[5] Comninou M, Schmueser D. The interface crack in a combined tension-compression and shear field. J App Mech 1979; 46:345–348.

[6] Gross D, Seelig T. Fracture Mechanics with the introduction to Micromechanics. Springer Heidelberg Dordrecht, New York; 2001.

[7] Tafreshi A. Computation of the J_k-integrals for bimaterial interface cracks using boundary element crack shape sensitivities. Theor App Fract Mech 2016; 82:77–87.

[8] Shiah YC, Hwu C, Yao JJ. Boundary element analysis of the stress intensity factors of plane interface cracks between dissimilarly adjoined anisotropic materials. Eng Anal Bound Elem 2019; 106:68–74.

[9] Menshykov OV, Menshykova MV, Wendland WL. On use of the Galerkin method to solve the fracture mechanics problem for a linear crack under normal loading. Int App Mech 2005; 41(11):1324–1329.

[10] Menshykova MV, Menshykov OV, Guz IA. An iterative BEM for the dynamic analysis of interface crack contact problems. Eng Anal Bound Elem 2011; 35(5): 735–749.

[11] Menshykov OV, Guz IA, Menshykov VA. Boundary integral equations in elastodynamics of interface cracks. Phil Trans R Soc A 2008;366(1871):1835–1839.

[12] Menshykova MV, Menshykov OV, Guz IA. Modelling crack closure for an interface crack under harmonic loading. Int J Fract 2010; 165(1):127–134.

[13] Menshykov OV, Menshykov VA, Guz IA. Elastodynamics of a crack on the bimaterial interface. Eng Anal Bound Elem 2009; 33(3):294–301.

[14] Men'shikov VA, Men'shykov AV, Guz IA. Interfacial crack between elastic half-spaces under harmonic loading. Int App Mech 2007; 43(8):865–873.

[15] Menshykov OV, Menshykova MV, Guz IA. 3-D elastodynamic contact problem for an interface crack under harmonic loading. Eng Fract Mech 2012; 80:52–59.

[16] Fomenko SI, Golub MV, Doroshenko OV, Wang Y, Zhang C. An advanced boundary integral equation method for wave propagation analysis in a layered piezoelectric phononic crystal with a crack or an electrode. J Comput Phys 2021;447:110669.

[17] Chan Y-S, Fannjiang AC, Paulino GH. Integral equations with hypersingular kernels – theory and applications to fracture mechanics. Int J Eng Sci 2003; 41:683–720.

[18] Zhang P, Du C, Zhao W, Sun L. Dynamic crack face contact and propagation simulation based on the scaled boundary finite element method. Comput Methods Appl Mech Eng 2021; 385:114044.

[19] Zhang P, Du C, Tian X, Jiang S. A scaled boundary finite element method for modelling crack face contact problems. Comput Methods Appl Mech Eng 2018; 328:431–451.

[20] Zhang P, Du C, Birk C, Zhao W. A scaled boundary finite element method for modelling wing crack propagation problems. Eng Fract Mech 2019; 216:106466.

[21] Jia Y-M, Li C-J ,Zhang Y, Chen J. The high-order completeness analysis of the scaled boundary finite element method. Comput Methods Appl Mech Eng 2020; 362:112867.

[22] Eskandari-Ghadi M, Ardeshir-Behrestaghi A, Pak RYS. Bi-material transversely isotropic half-space containing penny-shaped crack under time-harmonic horizontal loads. Eng Fract Mech 2017; 172:152–180.

[23] Mykhaskiv VV, Zhbadynskyi IYa, Zhang Ch. On propagation of time-harmonic elastic waves through a double-periodic array of penny-shaped cracks. Eur L Mech a Solids 2019; 73:306–317.

[24] Mykhaskiv VV, Zhbadynskyi IYa, Zhang Ch. Dynamic stresses due to time-harmonic elastic wave incidence on doubly periodic array of penny-shaped cracks. J Math Sci 2014; 203:114–122.

[25] Forsat M, Musharavati F, Eyvazian A, Demiral M, Khan A, Talebizadehsardari P, Babaei Mahani R, Mobayen S, Sebaey T. In-plane stress analysis of multiple parallel cracks in an orthotropic FGM medium under time-harmonic loading. Theor Appl Fract Mech 2021; 113:102936.

[26] Bagheri R, Enjilela V. Time-harmonic analysis of multiple interface cracks in two dissimilar FGM half-planes: In-plane problem. Theor Appl Fract Mech 2021; 116:103094.

[27] Bagheri R, Monfared MM. In-plane transient analysis of two dissimilar nonhomogeneous half-planes containing several interface cracks. Acta Mech 2020; 231:3779–3797.

[28] Bagheri R, Monfared MM. Mixed-mode fracture analysis for two dissimilar half-planes with multiple interface moving cracks. Waves Random Complex Media 2021; DOI: 10.1080/17455030.2021.1948147

[29] Jafari A, Monfared MM, Bagheri R. Mixed-mode computation of the transient dynamic stress intensity factor for multiple interface cracks. J Braz Soc Mech Sci 2019; 41:573.

[30] Rangelov T, Stoynov Y, Dineva P. Dynamic fracture behaviour of functionally graded magnetoelectroelastic solids by BIEM. Int J Solids Struct 2011; 48:2987–2999.

[31] Fan CY, Lv SY, Dang HY, Yuan YP, Zhao MH. Fundamental solutions and analysis of the interface crack for two-dimensional decagonal quasicrystal bimaterial via the displacement discontinuity method. Eng Anal Bound Elem 2019;106:462–472.

[32] Zhao MH, Fan CY, Lu C, Dang HY. Analysis of interface cracks in one-dimensional hexagonal quasi-crystal coating under in-plane loads. Eng Fract Mech 2021;243:107534.

[33] Petrova V, Schmaudera S, Ordyanc M, Shashkin A. Revisit of antiplane shear problems for an interface crack: Does the stress intensity factor for the interface

Mode III crack depend on the bi-material modulus. Eng Fract Mech 2019; 216:106524.

[34] Negi A, Singh AK, Yadav RP. Analysis on dynamic interfacial crack impacted by SH-wave in bi-material poroelastic strip. Compos Struct 2020; 233:111639.

[35] Vaysfeld N, Zhuravlova Z. The investigation of semi-strip's stress state with a longitudinal crack. ZAMM: Journal of Applied Mathematics and Mechanics 2020; DOI:10.1002/zamm.201900289

[36] Matbuly MS. Analytical solution for an interfacial crack subjected to dynamic anti-plane shear loading. Acta Mech 2006; 184:77–85.

[37] Wuensche M, Zhang Ch, Sladek J, Sladek V, Hirose S, Kuna M. Transient dynamic analysis of interface cracks in layered anisotropic solids under impact loading. Int J Fract 2009; 157:131–147.

[38] Zhang X, Shi Y, Pan G. Dynamic stress control of bi-material structure subjected to sawtooth shock pulse based on interface characteristics. Mech Res Commun 2020; 107:103558.

[39] Lira-Vergara E, Rubio-Gonzalez C. Dynamic stress intensity factor of interfacial finite cracks in orthotropic materials. Int J Fract 2005; 135:285–309.

[40] Basu S, Mandal SC. Impact of torsional load on penny-shaped crack in an elastic layer sandwiched between two elastic half-spaces. Int J Appl Comput 2016; 2:533–543.

[41] Karan S, Basu S, Mandal SC. Impact of a torsional load on a penny-shaped crack sandwiched between two elastic layers embedded in an elastic medium. Acta Mech 2018; 229:1759–1772.

[42] Itou S. Dynamic stress intensity factors around three parallel cracks in an infinite medium during a passage of impact normal stress. Acta Mech 2015; 226:2407–2420.

[43] Menshykova MV, Menshykov OV, Guz IA. Linear interface crack under plane shear wave. Comput Model Eng Sci 2009; 48(2):107–120.

[44] Guz AN, Guz IA, Men'shikov AV, Men'shikov VA. Penny-shaped crack at the interface between elastic half-spaces under the action of a shear wave. Int App Mech 2009; 45(5):534–539.

[45] Menshykov VA, Menshykov O, Guz IA. Contact problems for interface cracks under harmonic shear loading. Scipedia, V. 100 – Fracture, Damage and Failure Mechanics 2021. DOI:10.23967/wccm-eccomas.2020.104

[46] Zhang Ch, Gross D. On wave propagation in elastic solids with cracks. Computational Mechanics Publications; 1998.

[47] Guz AN, Zozulya VV. Elastodynamic unilateral contact problems with friction for bodies with cracks. Int App Mech 2002; 38:895–932.

[48] Guz AN. Nonclassical problems of fracture/failure mechanics: on the occasion of the 50th anniversary of the research (review). Int App Mech 2019; 55:129–174.

[49] Chai H, Bao Y, Zhang Z. Numerical solutions of hypersingular integral equations for interface circular crack under axisymmetric loadings. Eng Anal Bound Elem 2021; 122:35–42.

[50] Ostrik VI. Contact of faces of a rectilinear crack under complex loading and various contact conditions. Acta Mech 2019; 230:3741–3758.

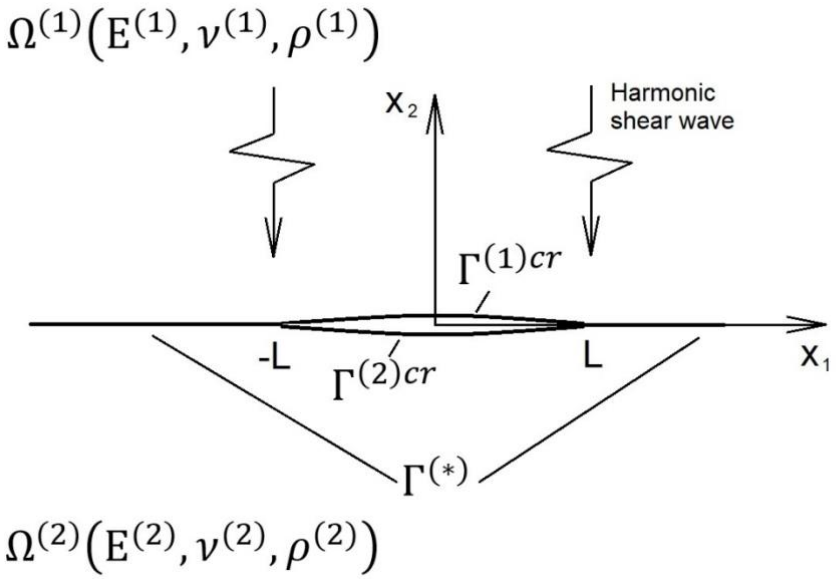

Figure 1: Interface crack under normal loading

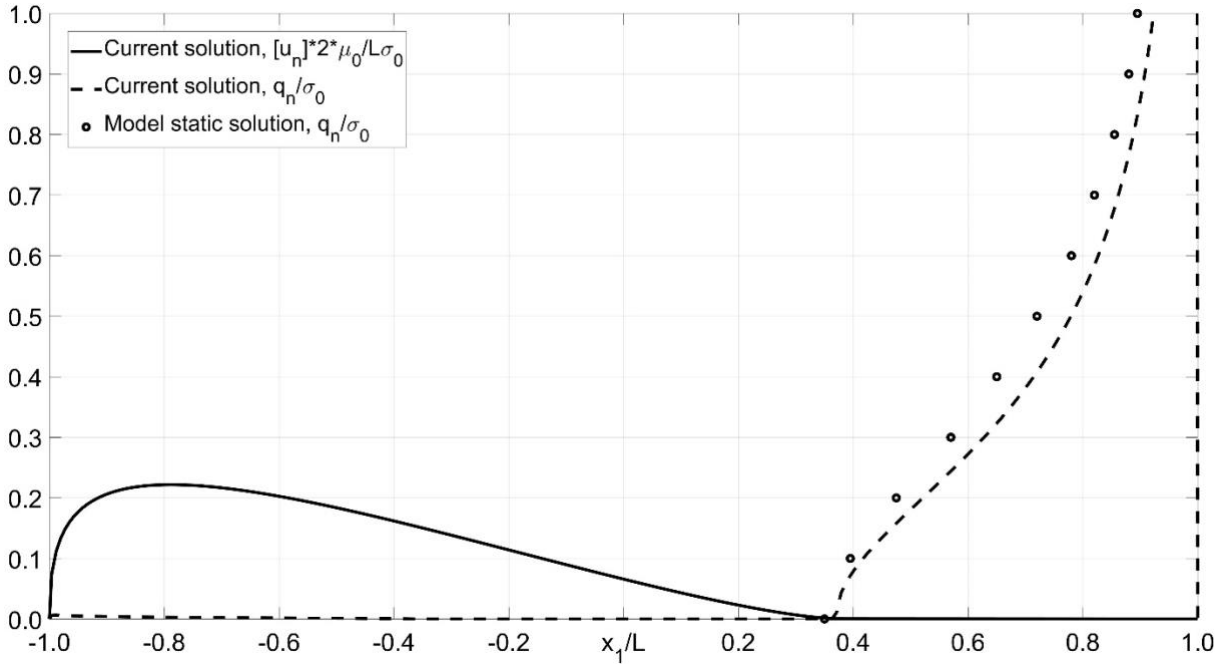

Figure 2: Normal components of the displacement jump and contact forces without friction, $k_\tau = 0.0$, adopted from [23]

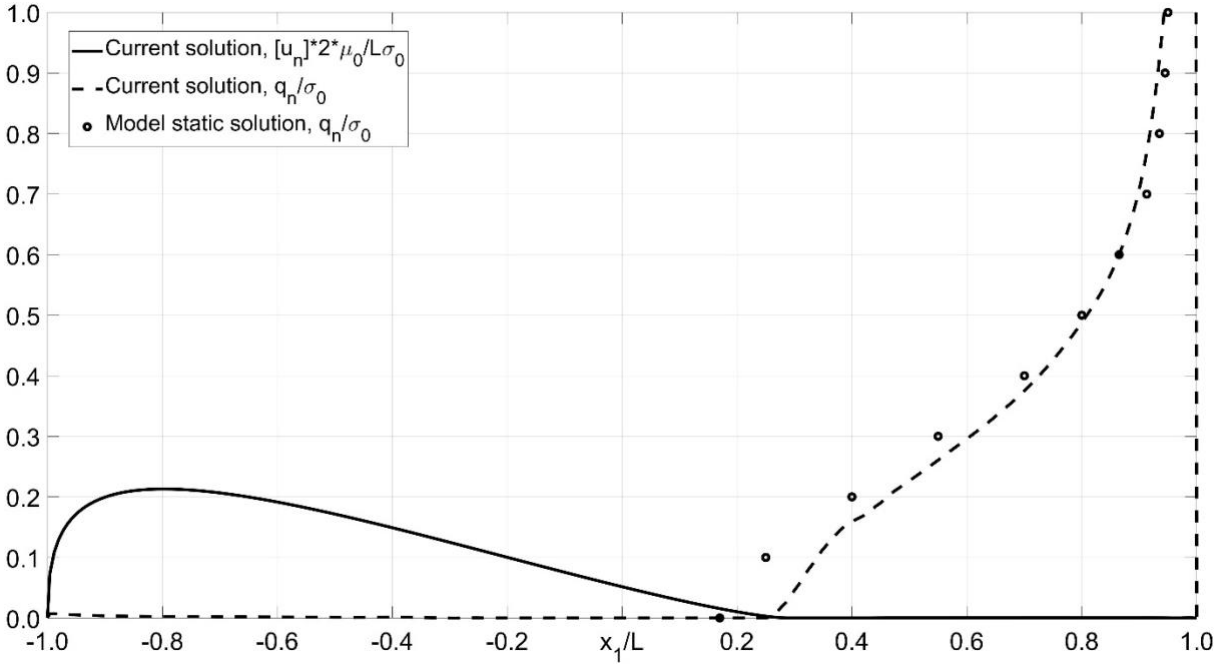

Figure 3: Normal components of the displacement jump and contact forces with friction, $k_\tau = 1.0$, adopted from [23]

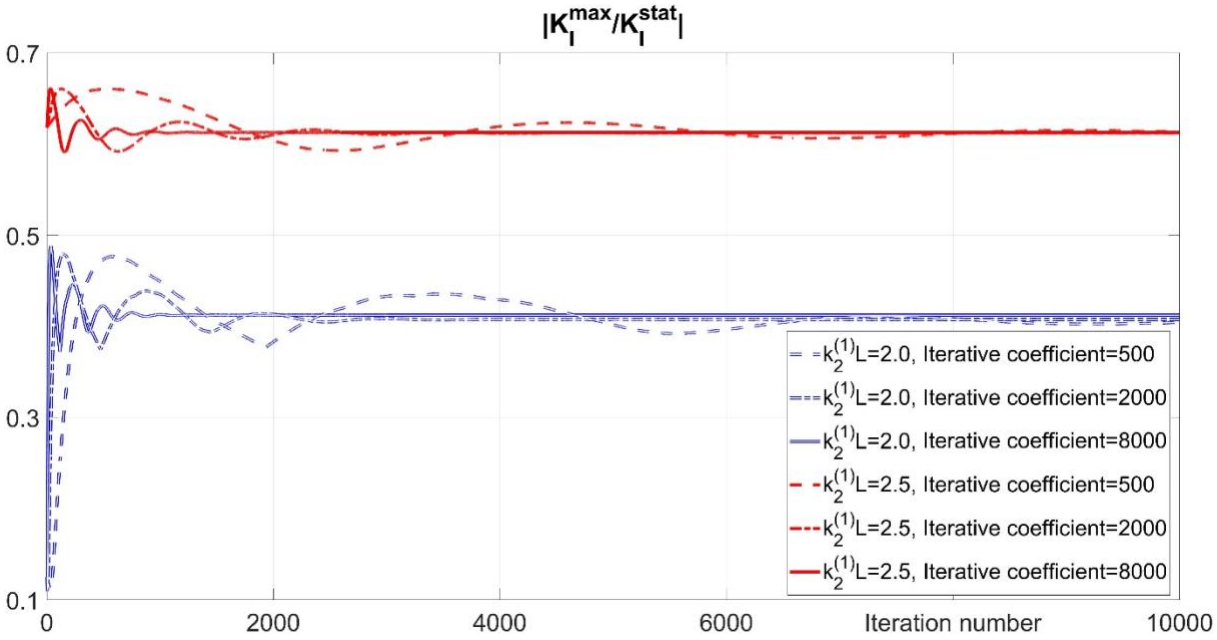

Figure 4: Stress intensity factor (normal opening mode) plotted against the iteration number for different wave numbers, $\mu^{(2)}/\mu^{(1)} = 0.5$, $k_\tau = 0.5$

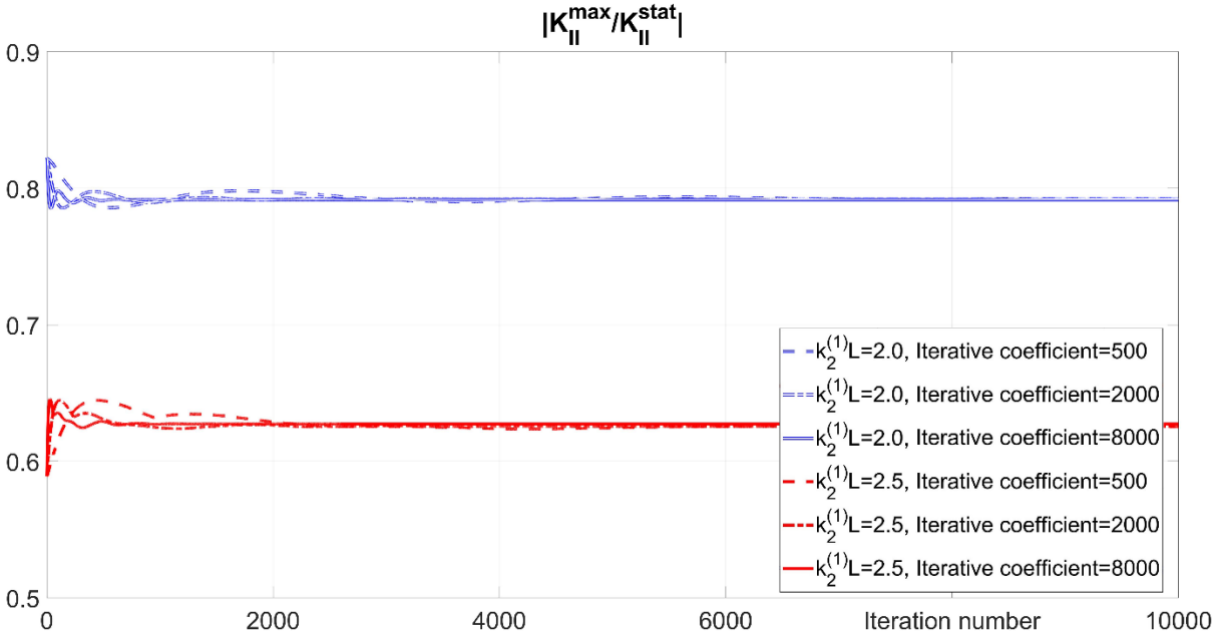

Figure 5: Stress intensity factor (transverse shear mode) plotted against the iteration number for different wave numbers, $\mu^{(2)}/\mu^{(1)} = 0.5$, $k_\tau = 0.5$

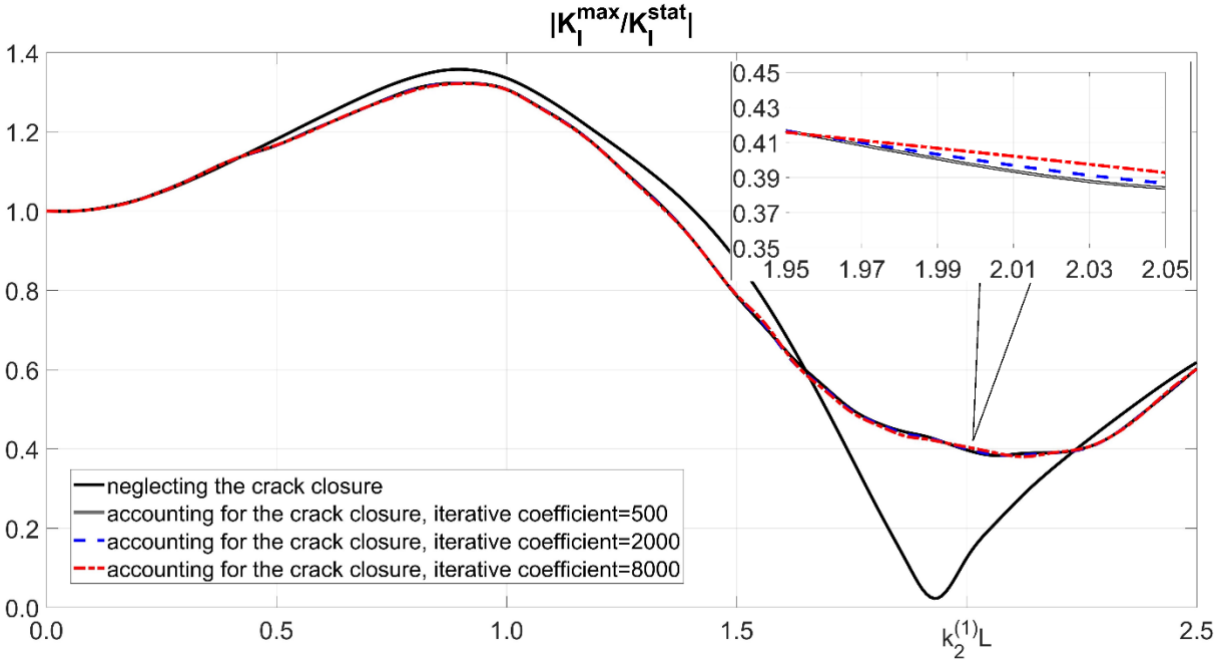

Figure 6: Stress intensity factor (normal opening mode) plotted against the wave number for different iterative coefficients, $\mu^{(2)}/\mu^{(1)} = 0.5$, $k_\tau = 0.5$

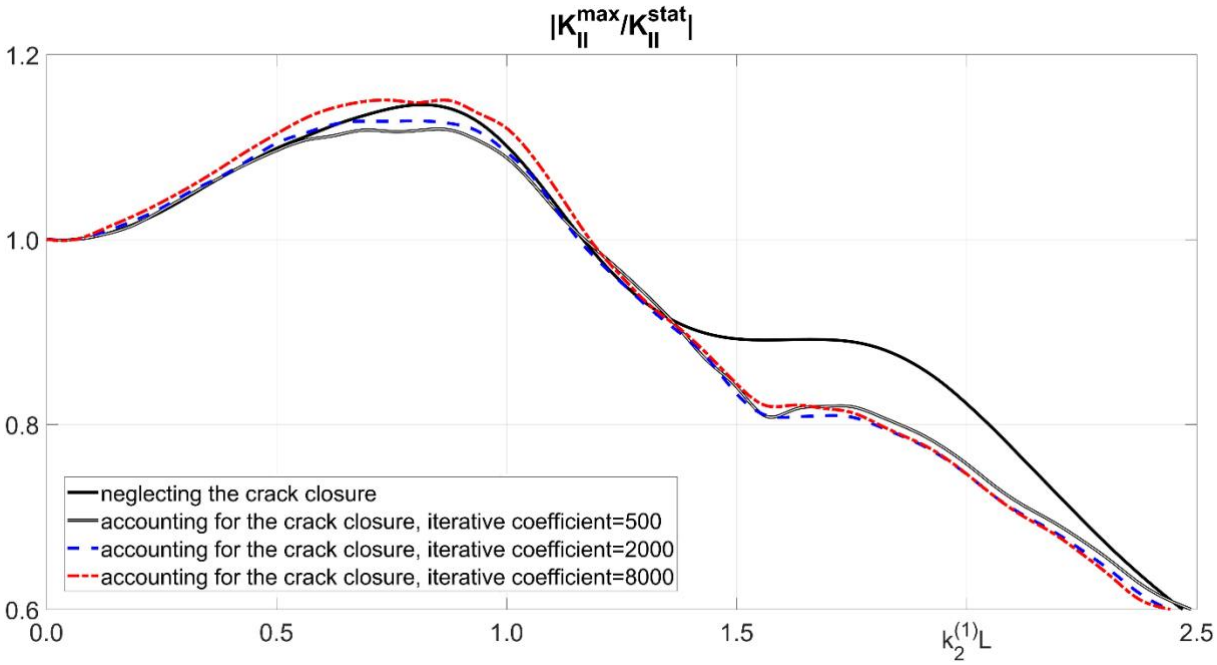

Figure 7: Stress intensity factor (transverse shear mode) plotted against the wave number for different iterative coefficients, $\mu^{(2)}/\mu^{(1)} = 0.5$, $k_\tau = 0.5$

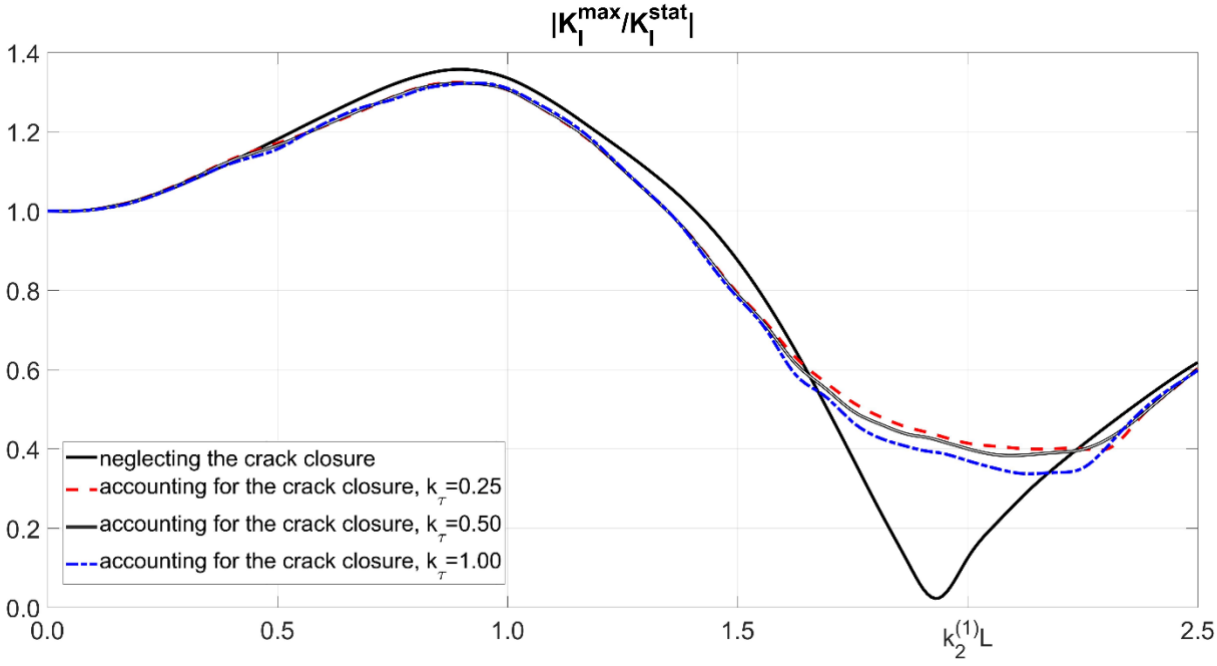

Figure 8: Stress intensity factor (normal opening mode) plotted against the wave number for different friction coefficients, $\mu^{(2)}/\mu^{(1)} = 0.5$, iterative coefficient 2000

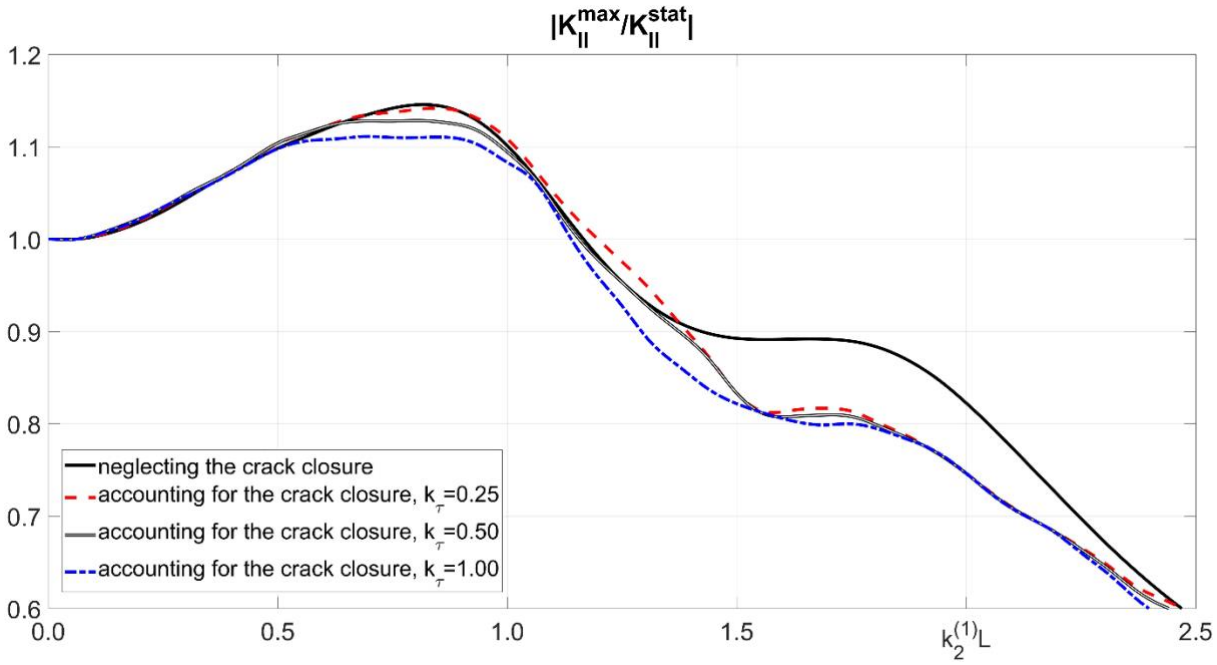

Figure 9: Stress intensity factor (transverse shear mode) plotted against the wave number for different friction coefficients, $\mu^{(2)}/\mu^{(1)} = 0.5$, iterative coefficient 2000

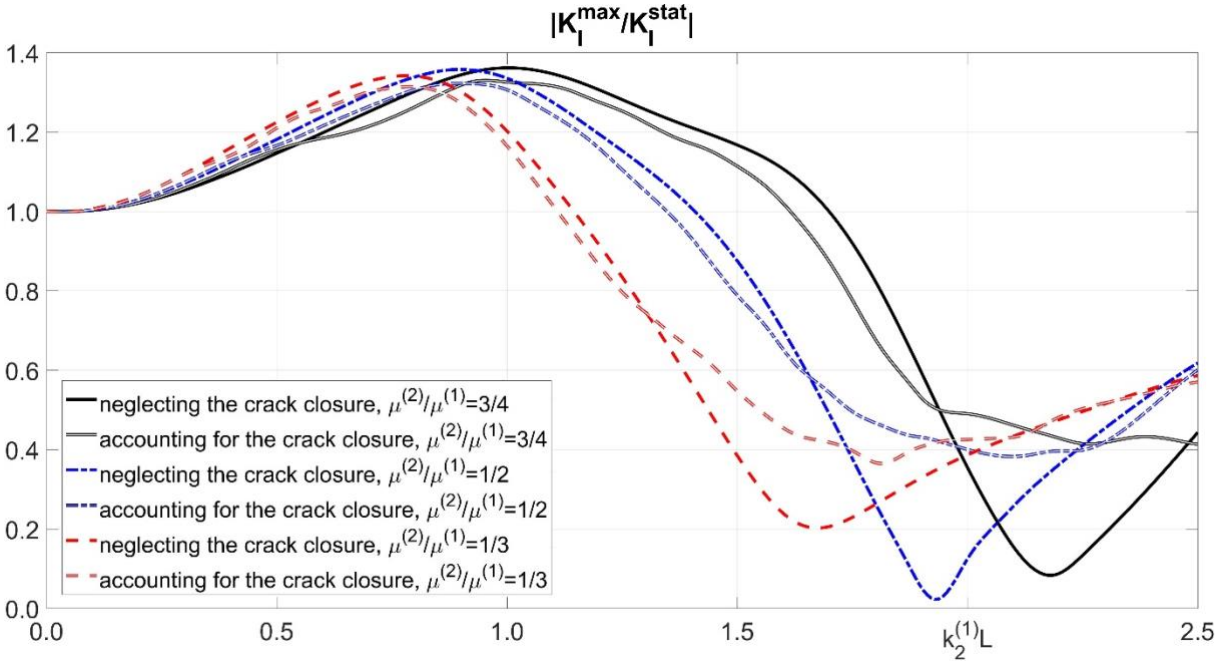

Figure 10: Stress intensity factor (normal opening mode) plotted against the wave number for different materials' properties, $k_\tau = 0.5$, iterative coefficient 2000

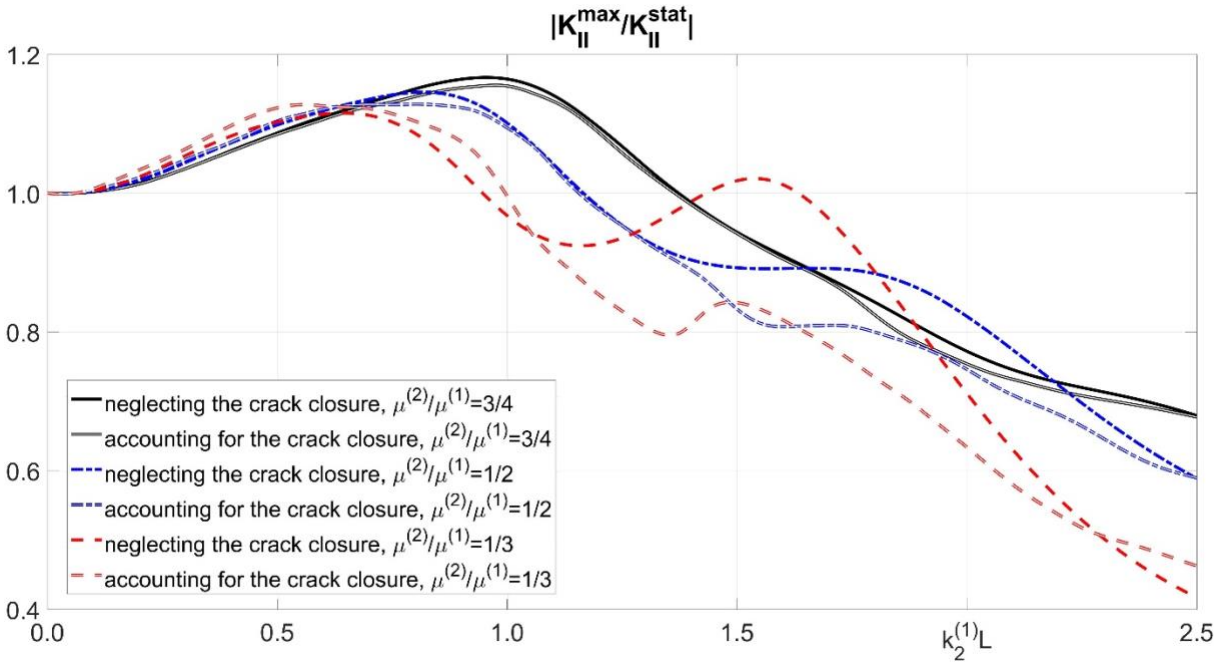

Figure 11: Stress intensity factor (transverse shear mode) plotted against the wave number for different materials' properties, $k_\tau = 0.5$, iterative coefficient 2000